AGU PUBLICATIONS

Geophysical Research Letters

RESEARCH LETTER
10.1002/2016GL070224

Key Points:
- Observations of magnetosheath ion intrusion into the magnetosphere ~9 ion skin depths downstream of an X line
- Magnetosheath ion Larmor radius effects in the magnetospheric inflow region indicate large-scale proximity to the X line
- Magnetosheath ion Larmor radius effects do not imply that a spacecraft is upstream of the electron diffusion region

Correspondence to:
T. D. Phan,
phan@ssl.berkeley.edu

Citation:
Phan, T. D., et al. (2016), Ion Larmor radius effects near a reconnection X line at the magnetopause: THEMIS observations and simulation comparison, *Geophys. Res. Lett.*, *43*, 8844–8852, doi:10.1002/2016GL070224.

Received 28 JUN 2016
Accepted 10 AUG 2016
Accepted article online 11 AUG 2016
Published online 2 SEP 2016

Ion Larmor radius effects near a reconnection X line at the magnetopause: THEMIS observations and simulation comparison

T. D. Phan[1], M. A. Shay[2], C. C. Haggerty[2], J. T. Gosling[3], J. P. Eastwood[4], M. Fujimoto[5], K. Malakit[6], F. S. Mozer[1], P. A. Cassak[7], M. Oieroset[1], and V. Angelopoulos[8]

[1]Space Sciences Laboratory, University of California, Berkeley, California, USA, [2]Department of Physics and Astronomy, University of Delaware, Newark, Delaware, USA, [3]Laboratory for Atmospheric and Space Physics, University of Colorado Boulder, Boulder, Colorado, USA, [4]The Blackett Laboratory, Imperial College London, London, UK, [5]ISAS/JAXA, Kanagawa, Japan, [6]Department of Physics, Mahidol University, Bangkok, Thailand, [7]Department of Physics and Astronomy, West Virginia University, Morgantown, West Virginia, USA, [8]Department of Earth, Planetary, and Space Sciences, University of California, Los Angeles, California, USA

Abstract We report a Time History of Events and Macroscale Interactions during Substorms (THEMIS-D) spacecraft crossing of a magnetopause reconnection exhaust ~9 ion skin depths (d_i) downstream of an X line. The crossing was characterized by ion jetting at speeds substantially below the predicted reconnection outflow speed. In the magnetospheric inflow region THEMIS detected (a) penetration of magnetosheath ions and the resulting flows perpendicular to the reconnection plane, (b) ion outflow extending into the magnetosphere, and (c) enhanced electron parallel temperature. Comparison with a simulation suggests that these signatures are associated with the gyration of magnetosheath ions onto magnetospheric field lines due to the shift of the flow stagnation point toward the low-density magnetosphere. Our observations indicate that these effects, ~2–3 d_i in width, extend at least 9 d_i downstream of the X line. The detection of these signatures could indicate large-scale proximity of the X line but do not imply that the spacecraft was upstream of the electron diffusion region.

1. Introduction

Reconnection at Earth's magnetopause typically involves asymmetric inflow densities on the two sides of the current sheet [e.g., *Paschmann et al*., 1979; *Sonnerup et al*., 1981], with the magnetosheath density higher than the magnetospheric density, typically by a factor of 10 or more. A consequence of this large asymmetry is that in the reconnecting current sheet, the stagnation point is shifted toward the magnetospheric side [e.g., *Cassak and Shay*, 2007; *Eastwood et al*., 2013], and the location of the peak reconnection jet speed in the exhaust is skewed toward the magnetosphere [e.g., *Gosling et al*., 1991; *Phan et al*., 1996].

In the downstream exhaust, the reconnection outflow is confined to the current sheet [*Paschmann et al*., 1979; *Sonnerup et al*., 1981]. However, near the X line, the current sheet width is at its thinnest and the distance from the stagnation point to the magnetospheric edge (i.e., where the magnetic field begins to rotate) could be smaller than the gyroradii of magnetosheath ions. A recent simulation by *Shay et al*. [2016] showed that this leads to the penetration of magnetosheath ions into the magnetosphere near the X line. Higher-energy ions penetrate deeper, leading to a Larmor radius effect. Due to their smaller gyroradii, magnetosheath electrons cannot penetrate into the magnetosphere as deeply as the ions.

In the simulation, the Larmor radius effect was found to occur within ~15 ion skin depths (d_i) of the X line in the downstream direction. Farther downstream, the radial distance from the stagnation point to the magnetosphere is larger than the gyroradii of magnetosheath ions such that magnetosheath ions are mostly confined to the current sheet. Furthermore, due to the time-of-flight effect, field-aligned magnetosheath electrons penetrate deeper into the magnetosphere than field-aligned ions [e.g., *Gosling et al*., 1990; *Khotyaintsev et al*., 2006; *Oieroset et al*., 2015]. This is opposite to the ion gyroradius effect near the X line.

Because of the localization of this magnetosheath ion Larmor radius effect, *Shay et al*. [2016] suggested that this signature could be used to provide large-scale context for spacecraft encounters of the dayside reconnection X line region. This would be particularly useful for crossings that are normal to the current sheet, as opposed to crossings along the outflow direction, where bidirectional jet signatures could provide

the context for the identification of the X line region [e.g., *Phan et al*., 2003; *Wilder et al*., 2014; *Burch et al*., 2016; *Phan et al*., 2016]. Recently, *Khotyaintsev et al*. [2016] and *Burch and Phan* [2016] reported signatures of magnetosheath ion penetration and electron parallel heating in the magnetospheric inflow region within 1–2 d_i of the X line.

In this paper, we describe a comprehensive analysis of a Time History of Events and Macroscale Interactions during Substorms (THEMIS-D) crossing of the dayside magnetopause that exhibits many of the predicted properties associated with the Larmor radius effect in the magnetospheric inflow region. The observations are compared with a simulation based on the observed inflow conditions. Our findings suggest that magnetosheath ion Larmor radius effects extend at least 9 d_i downstream of the X line.

2. Simulation

In this section, we describe the large (ion)-scale plasma and field structures surrounding the X line based on a 2.5-D particle-in-cell (PIC) simulation, with emphasis on features that can be compared with the THEMIS observations. The simulation uses inflow parameters that correspond to the THEMIS nearly antiparallel reconnection event to be discussed: the magnetosheath inflow region was initialized with a magnetic field of 30 nT, a proton density of 15 cm^{-3}, and ion and electron temperatures of 270 and 40 eV, respectively. The magnetospheric inflow region had a magnetic field of 50 nT, density of 0.45 cm^{-3}, and ion and electron temperatures of 1400 eV and 52 eV, respectively. With these parameters, the total pressure is uniform across the magnetopause current sheet.

The simulation parameters and boundary conditions are somewhat similar to those of *Malakit et al*. [2013] and *Shay et al*. [2016], but there are differences as well. The main differences are the much larger ion temperature ratio across the magnetopause and larger ion-to-electron temperature ratio in the magnetosphere. This leads to clearer signatures of the escape of magnetospheric ions near the magnetopause current sheet not noted in the previous studies. Furthermore, the new simulation reveals that the "Larmor electric field," which was thought to be localized near the X line, actually extends more than 35 d_i downstream. On the other hand, signatures of magnetosheath ion gyroradius effects are more localized and therefore better indicators of the proximity to the X line. Details of the simulation setup can be found in the Appendix A. The simulation results are presented in physical units to allow for quantitative comparison with THEMIS observations.

Figure 1 shows the plasma and field structures of the reconnecting current sheet and its upstream regions, with the magnetosheath at the top and the magnetosphere at the bottom of the panels. The simulation results are shown in the *LMN* coordinate system, with *N* pointing along the overall current sheet normal (upward), *M* along the X line direction (into the plane), and *L* along the outflow direction (positive to the right). In the figure, the separatrices are the field lines that converge at the X point. The region of interest is the magnetospheric inflow region near the X line. Within ~±15 d_i of the X line (in the ±*L* directions), the ion outflow (v_{iL}) jet extends beyond the magnetospheric separatrix into the magnetosphere (Figure 1d). In the same region, there is a strong negative (out-of-plane, blue) ion flow v_{iM} (Figure 1e) and a large enhancement of the electron parallel temperature (Figure 1i). There is no significant intrusion of the electron outflow (v_{eL}) jet into the magnetospheric inflow region (Figure 1f). Farther downstream, the ion outflow and the negative v_{iM} are inward of the separatrix, and no parallel electron heating is seen in the magnetospheric inflow region.

The intrusion of the ion flow into the magnetosphere is due to the penetration of magnetosheath ions. The fact that there is no intrusion from the electron flow indicates that this is an ion Larmor radius effect [*Shay et al*., 2016]. Figures 2d and 2e display the ion distributions in the magnetosheath ion intrusion region (sampled in rectangular boxes in Figure 2a), which show the Larmor gyroradius signatures and the resulting net out-of-plane drift (i.e., $v_{iM} < 0$) of the ions. The sketch in Figure 2b explains this effect where magnetosheath ions (in blue orbits) penetrate into the magnetosphere and perform a partial Larmor orbit. The net negative v_{iM} is due to the imbalance of magnetosheath and magnetospheric ion density in this region (with magnetosheath density ≫ magnetospheric density).

The lack of magnetosheath electron penetration into the magnetosphere is attributed to their smaller gyroradii. *Shay et al*. [2016] suggested that in order to achieve charge neutrality in the region of excess ions,

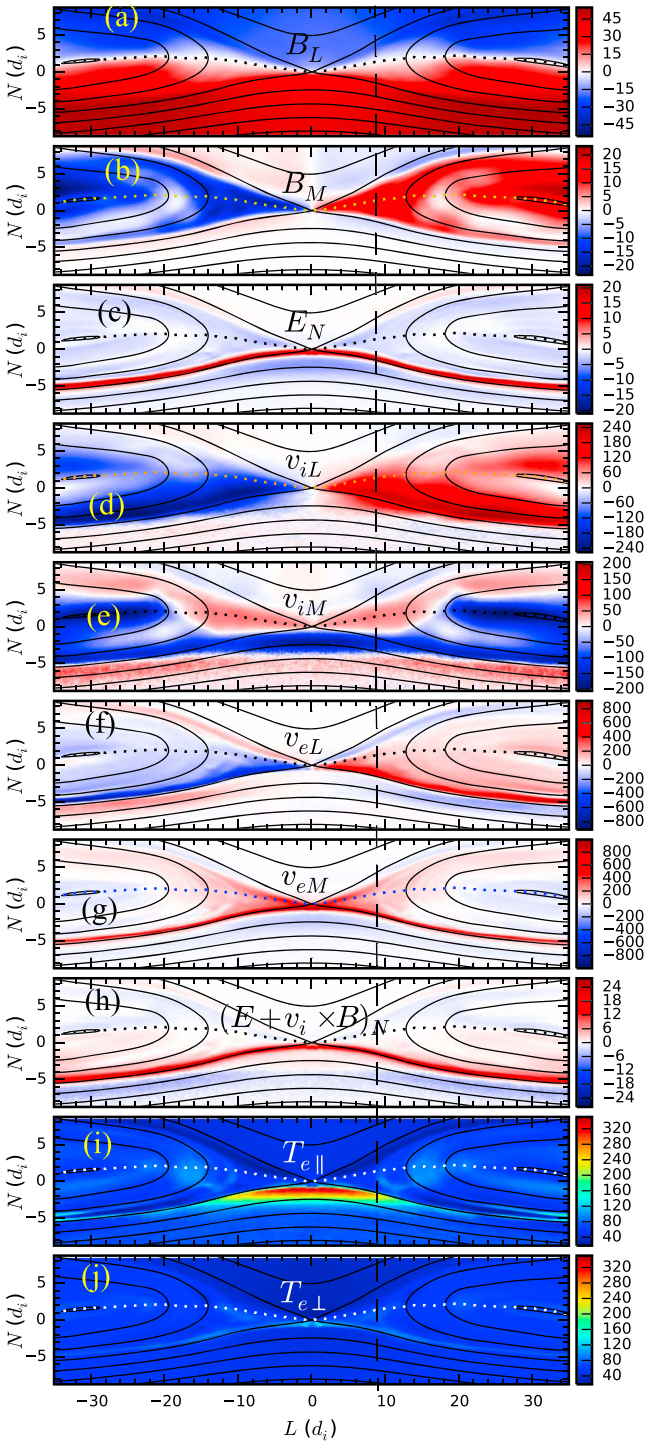

Figure 1. Simulation results in the *L*-*N* plane in ion inertial units. The positive *M* direction is into the plane. (a) Reconnecting field component, (b) into-the-plane magnetic field, (c) normal electric field, (d) ion outflow velocity, (e) into-the-plane ion velocity, (f) electron outflow velocity, (g) into-the-plane electron velocity, (h) ion frozen-in condition along *N*, and (i, j) electron parallel and perpendicular temperatures.

magnetospheric electrons are drawn into the region by parallel electric fields, resulting in a large parallel electron temperature increase seen in that region. The fact that parallel electron heating (Figure 1i) occurs in precisely the same region as the ion intrusion (Figure 1e) indicates that the magnetosheath ion intrusion into the magnetosphere and the electron heating in the same region are intimately related. The parallel electric fields and electron heating are also present in the *Egedal et al.* [2011] model. That model did not relate the electron heating and parallel electric field to the magnetosheath ion gyroradius effect, although an excess of plasma density in the magnetosphere near the X line (relative to the downstream region) present in the model could be consistent with magnetosheath ion penetration into the magnetosphere.

A feature that was not noted in previous simulations by *Malakit et al.* [2013] and *Shay et al.* [2016] is the into-the-plane ($v_{iM} > 0$, red) flow in the magnetosphere (Figure 1e). Well downstream of the X line ($|L| > 20\ d_i$) this flow is seen next to the magnetospheric separatrix. Closer to the X line, the positive (red) v_{iM} flow is weaker and is located earthward of the negative v_{iM} region and farther from the separatrix. Examination of the ion distributions in this region (Figure 2f) shows that the positive v_{iM} is associated with a magnetospheric ion Larmor radius effect. Magnetospheric ions, whose orbits intersect the current sheet and the sunward pointing normal electric field (E_N), do not return to the magnetosphere (as illustrated in the sketch in Figure 2b). The loss of such particles results in a net positive v_{iM} flow (Figure 2f).

Just upstream of the magnetospheric separatrix, there is a region of negative (earthward pointing) E_N (Figure 1c) previously termed the Larmor electric field [*Malakit et al.*, 2013]. This E_N is largest near the X line, but it extends beyond $L = 35\ d_i$ in the present

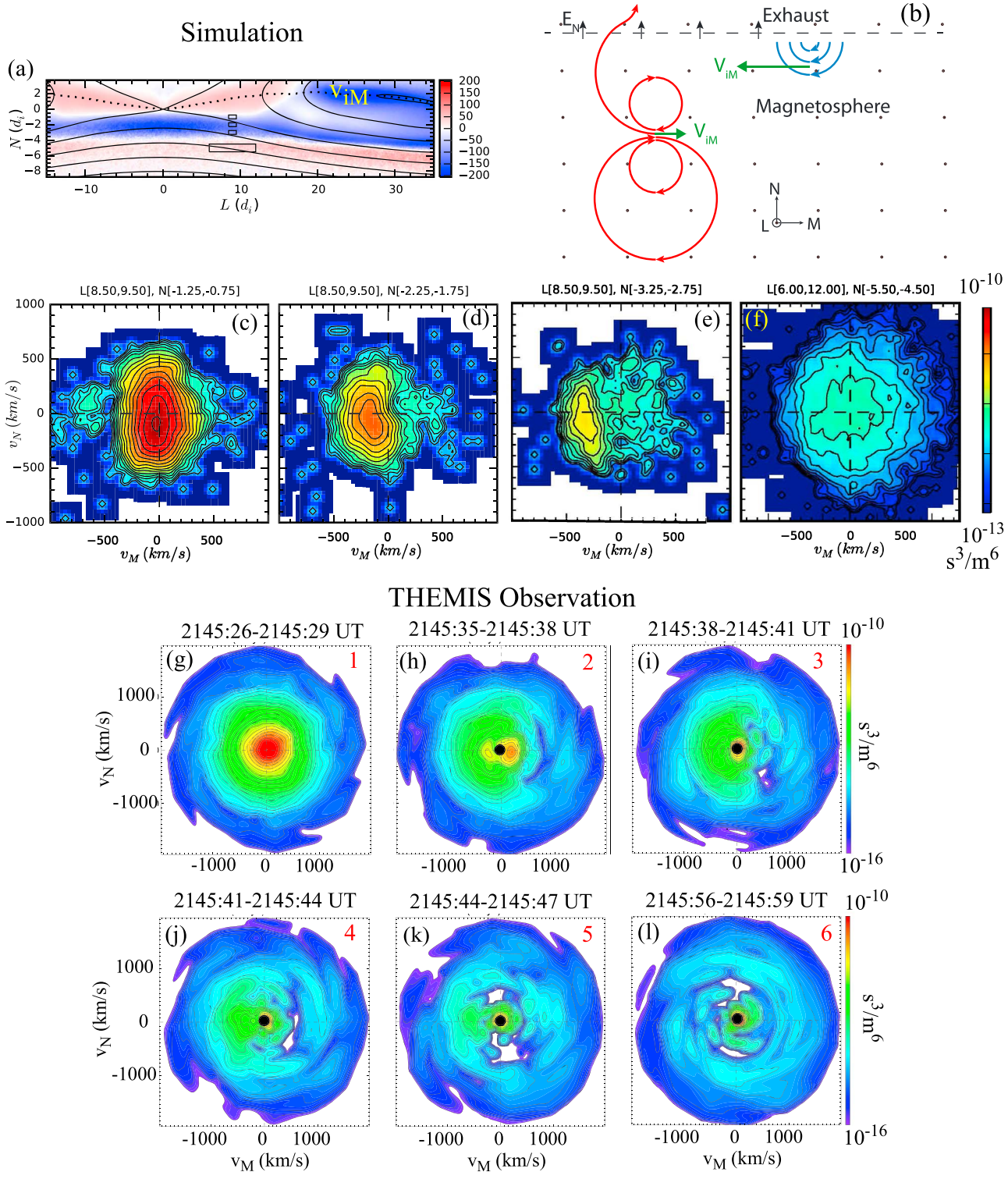

Figure 2. The 2-D cuts of 3-D Ion distributions around the magnetospheric inflow regions in the *M-N* plane, which is close to the plane perpendicular to the magnetospheric magnetic field. Figures 2c–2f are from simulations, while Figures 2g–2l are from THEMIS-D observations at the locations labeled "1" to "6" at the bottom of Figures 3a–3l. (a) Structure of into-the-plane velocity v_{iM}, with boxes showing sampling locations used to create ion distribution functions in Figures 2c–2f, (b) schematic of magnetosheath (blue) and magnetospheric (red) ion orbits near the magnetospheric edge of the current sheet and the resulting net v_{iM} (green), (c) ion distribution in the exhaust, (d, e) ion distributions in the negative v_{iM} region showing a magnetosheath ion Larmor radius effect, (f) ion distribution in the positive v_{iM} region showing loss of high-energy magnetospheric ions on the negative v_M side, (g) observed exhaust ion distribution, (h–k) observed ion distributions in the $v_{iM} < 0$ region showing the magnetosheath ion Larmor radius effect, and (l) observed ion distribution in the region of positive v_{iM}.

simulation. *Malakit et al*. [2013] suggested that this field is associated with magnetospheric ion Larmor radius effects, while *Shay et al*. [2016] suggested that it is associated with magnetosheath ion Larmor radius effects instead. The fact that this negative E_N region extends far beyond the region where the magnetosheath ion intrusion occurs indicates that this field is not associated with magnetosheath ion Larmor radius effects alone. It is likely to be due to a combination of magnetosheath and magnetospheric ion Larmor radius effects. Finally, the fact that the $E_N < 0$ region in the magnetosphere extends beyond $|L| = 35\ d_i$, while the magnetosheath ion gyroradius effects are localized to $|L| \sim 15\ d_i$, suggests that the latter are a better indicator of the proximity to the X line.

3. Observations

The present study uses 3 s resolution plasma [*McFadden et al*., 2008] and magnetic field [*Auster et al*., 2008] data and eight samples/second electric field data [*Bonnell et al*., 2008] from the THEMIS-D spacecraft. The data are shown in *LMN* boundary normal coordinates similar to the simulation coordinates (Figure 1), with *N* along the magnetopause normal, *L* along the reconnecting field direction, and *M* approximately along the X line direction.

Figures 3a–3l show the inbound magnetopause crossing of interest made by the THEMIS-D spacecraft on 9 September 2008 at 21:45 UT near the subsolar point (12.3 magnetic local time). The current sheet (i.e., magnetic field rotation region) is contained between the two black vertical dashed lines. Because the field rotation on the magnetospheric edge of the magnetopause was gradual, it is difficult to precisely mark the end of magnetic field rotation. However, a well-defined marker for this edge (in the observation as well as in the simulation) is the location of peak sunward pointing normal electric field, $E_N > 0$ (Figures 3k and 3s). According to the simulation (Figure 1c), within ~35 d_i of the X line, the peak E_N nearly coincides with the magnetospheric separatrix. In the THEMIS-D event, at the peak E_N location, marked by the third vertical dashed line, the magnetic field has completed more than 95% of its rotation from the magnetosheath to the magnetospheric orientation. The full magnetic field rotation across the magnetopause was ~174°; i.e., the guide field was close to zero.

An ion jet directed in the +*L* direction with speed ~120–170 km/s (relative to the magnetosheath flow) was detected throughout the current sheet (Figure 3f) and past the peak E_N location (Figure 3k). Figure 3g shows that the observed jet speed (in blue) was substantially lower than the predicted jet speed (in black) based on the Walén relation [*Paschmann et al*., 1986, equation (7)]. This is an indication that THEMIS-D crossed the reconnection exhaust relatively close to the X line, at a location where the ion outflow had not yet reached its full speed.

A magnetopause normal speed v_N of 14.0 km/s was obtained using the Minimization of the Faraday Residue method [*Khrabrov and Sonnerup*, 1998] for the 21:45:13–21:45:32 UT interval surrounding the magnetopause current sheet (between the two black dashed lines in Figures 3a–3l). With the current sheet crossing duration of 19 s, the width of the current sheet was ~266 km or ~4.5 ion skin depths based on the magnetosheath density of 15 cm^{-3}.

The distance of the observation point to the X line can be estimated using the simulation result (Figures 1a–1j). In the simulation, an exhaust width of 4.5 d_i occurs at $|L| \sim 9\ d_i$ downstream of the X line.

A unipolar positive magnetic field B_M was observed inside the current sheet (Figure 3b). The direction of this field is consistent with the bipolar Hall magnetic field expected for highly asymmetric reconnection (Figure 1b) [e.g., *Tanaka et al*., 2008] (as opposed to quadrupolar Hall field for symmetric reconnection [e.g., *Sonnerup*, 1979]). A normal electric field was observed at the magnetospheric edge of the magnetopause current sheet (Figure 3k). The location and direction of this field is consistent with the Hall electric field for asymmetric reconnection (Figure 1c) [*Vaivads et al*., 2004; *André et al*., 2004]. The ions were not frozen in ($E_N \neq -(\mathbf{v}_i \times \mathbf{B})_N$) in this region.

The electron spectrogram (Figure 3d) shows that magnetosheath electrons did not penetrate as deep into the magnetosphere as the ions (Figures 2k and 3c): magnetosheath ions were observed until 2145:47 UT, whereas magnetosheath electrons stopped at 2145:38 UT (the following electron sample, till 2145:41 UT, shows low- and high-energy magnetospheric electrons, but no magnetosheath electrons). This suggests that magnetosheath electrons were unable to penetrate as deeply into the magnetosphere as magnetosheath ions, similar to the simulation.

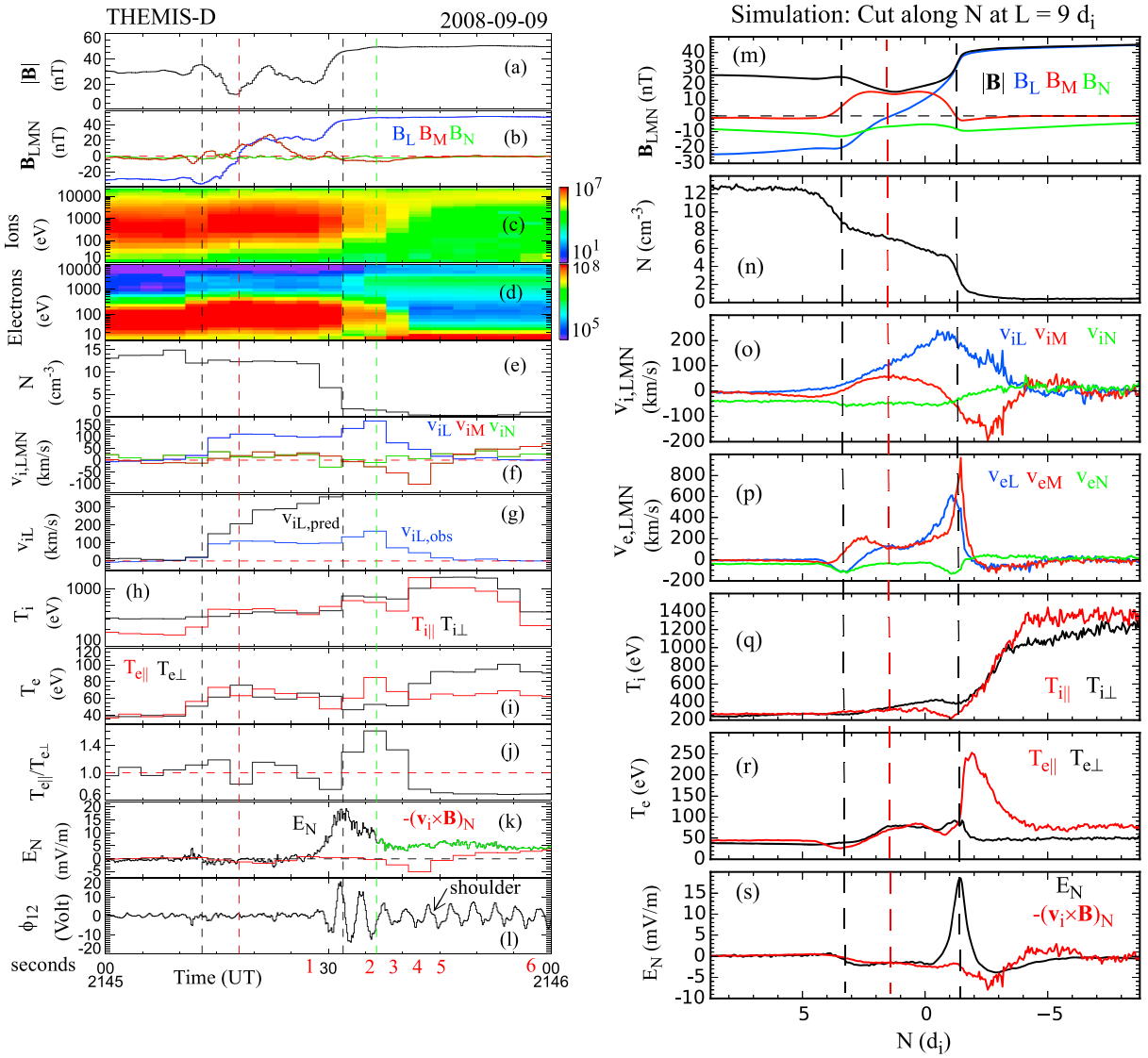

Figure 3. THEMIS crossing of a reconnecting magnetopause ~9 d_i downstream of the X line in *LMN* coordinates and comparison with simulation. (a) Magnetic field strength, (b) magnetic field, (c, d) ion and electron spectrograms of differential energy flux (eV s^{-1} cm^{-2} sr^{-1} eV^{-1}), (e) ion density, (f) ion velocity, (g) observed and predicted (from the Walen relation) *L* component of the velocity, (h) ion temperature, (i) electron temperature, (j) electron temperature anisotropy, (k) normal component of the electric field and $-\mathbf{v}_i \times \mathbf{B}$, and (l) potential between electric field probe 1 and probe 2. The two black vertical dashed lines in Figures 3a–3l mark the edges of the current sheet. The red dashed line denotes $B_L = 0$. The electric field data (Figure 3k) is unreliable to the right of the green vertical dashed line because of cold ion wake effect shown in Figure 3l. Figures 3m–3s show 1-D spatial profiles along *N* at $L = 9$ d_i of the simulation in Figure 1. (m) Magnetic field, (n) electron density, (o, p) ion and electron velocities, (q) ion temperatures, (r) electron temperatures, and (s) normal electric field and $-\mathbf{v}_i \times \mathbf{B}$.

4. Detailed Comparison of Observations and Simulation

We now compare in more detail the observed plasma and field profiles (Figures 3a–3k) with the simulation profiles at $L = 9$ d_i (Figures 3m–3s) and the measured and simulated ion distributions shown in Figure 2.

The spacecraft detected several predicted signatures of magnetosheath ion Larmor effects in the magnetosphere in close proximity to the magnetopause (located to the right of the last black vertical dashed line). These signatures include (a) ion energy dispersion, with high-energy ions being able to penetrate deeper into the magnetosphere (Figure 3c); (b) the intrusion of the outflow jet v_{iL} into the magnetospheric inflow region, past the E_N peak (Figure 3f); (c) enhanced out-of-plane velocity ($v_{iM} < 0$) (Figure 3f); and (d) enhanced electron parallel temperature (Figure 3i) and field-aligned temperature anisotropy (Figure 3j). Note that in both the simulations and the observations, the electron and ion β are substantially less than unity in the region of large

parallel temperature anisotropy, making this region stable to the firehose instability. Figures 2h–2k show that the negative v_{iM} is associated with ion distributions having a cutoff on the positive v_M side, consistent with the magnetosheath ion Larmor radius effect seen in the simulation (Figures 2d and 2e). The net negative v_{iM} is due to the fact the density of the penetrating magnetosheath ions is much higher than the density of magnetospheric ions at this location. Such dynamics do not occur in symmetric reconnection.

Earthward of the negative v_{iM} region in the magnetosphere, THEMIS-D observed a positive v_{iM} (Figure 3f), which is similar to the magnetospheric ion gyroradius effect seen in the simulation (Figures 1e and 3o). v_{iM} returned to zero at ~2146:12 UT (outside the time range of the figure). The loss of high-energy magnetospheric ions on the $-v_M$ side (compared to the $+v_M$ side) may be present in the observed ion distribution (Figure 2l), but it is not as clear as in the simulation (Figure 2f).

The observed amplitude of B_M relative to B_L (Figure 3b) is similar to the simulation (Figure 3m). The observed negative v_{iM} peak occurring earthward (to the right) of the peak of v_{iL} (Figure 3f) and peak $T_{e||}$ (Figure 3i) is similar to the simulation (Figures 3o and 3r) as well. The observed amplitude of the positive E_N of ~18 mV/m and of $-(\mathbf{v}_i \times \mathbf{B})_N$ of −5 mV/m (Figure 3k) is remarkably similar to the simulation (Figure 3s). Finally, the observed region of negative v_{iM} (Figure 3f) spanned ~9–12 s or 170 km. This corresponds to ~2–3 d_i (based on the magnetosheath density of 15 cm^{-3}), also consistent with the simulation (Figure 3o). It is also comparable to the ~200 km gyroradii of the highest-energy (~5 keV) exhaust ions (Figures 3c and 2h–2k) in a 50 nT magnetospheric magnetic field.

A major difference between the observations and the simulations is the lack of observed negative E_N (also known as the Larmor electric field) in the magnetospheric inflow region (Figure 3k) that is seen in the simulation (Figure 3s). However, upon closer examination of the electric field data, it is found that the electric field measurements are erroneous after 2145:36.5 UT (to the right of the vertical green dashed line) in the magnetospheric inflow region where a negative E_N is predicted. This is due to the cold ion wake effect behind the spacecraft that occurs in the low-density magnetosphere. A signature of the wake effect is the "shoulder" seen in the electric field probe-to-probe potential (Figure 3l) [*Eriksson et al*., 2006]. In other words, E_N in this region is not trustworthy. While the predicted negative E_N was not measured by the electric field experiment, the normal component of $-\mathbf{v}_i \times \mathbf{B}$ in this region was negative (Figure 3k), similar to that in the simulation (Figure 3s). Furthermore, the ion measurements described above clearly reveal the magnetosheath ion gyroradius effect in the magnetospheric inflow region.

Another discrepancy is the ion outflow speed. The observed outflow velocity v_{iL} in the exhaust and in the magnetospheric inflow region was ~100–170 km/s (Figure 3f), whereas in the simulation at $L \sim 9$ d_i, the outflow speed was much higher, reaching 220 km/s (Figure 3o). Furthermore, the observed v_{iL} peak occurred in the inflow region, earthward of the peak E_N location, whereas the v_{iL} peak in the simulation occurs in the exhaust, sunward of peak E_N. These discrepancies are currently not understood.

5. Summary and Discussions

We have examined a THEMIS-D crossing of the reconnecting magnetopause, where the observed exhaust outflow speed was substantially below the predicted reconnection outflow speed, suggesting that the crossing was relatively close to the X line. In the magnetospheric inflow region, THEMIS observed signatures of magnetosheath ion intrusion into the magnetosphere that were predicted by simulations to occur within 15 d_i downstream of the X line. The downstream distance of the THEMIS-D crossing of the exhaust is estimated to be ~9 d_i by finding the location in the simulation where the exhaust width matches that of the observed width of 4.5 d_i. However, if we estimate the distance by assuming a constant exhaust opening angle of 11° (corresponding to a reconnection rate of 0.1), that would put the spacecraft 22.5 d_i downstream of the X line. The vastly different estimates from the two methods may be due to the fact that the assumption of constant opening exhaust angle is not valid close to the X line for asymmetric reconnection (Figure 1). The detection of magnetosheath ion Larmor effects 9 d_i downstream from the X line is consistent with the simulation (Figures 1a–1j), whereas 22.5 d_i downstream is not. In the simulation these effects do not extend beyond $|L| \sim 15$ d_i. The observed depth of the magnetosheath ion intrusion was 2–3 magnetosheath ion skin depths or about one gyroradius of the highest-energy (~5 keV) exhaust ions.

Did the spacecraft cross the electron diffusion region? The simulation in section 2 (and discussed in more detail in *Shay et al*. [2016]) revealed a simple way to recognize the electron diffusion region, namely, the presence of $E_N > 0$ at the current sheet center ($B_L = 0$). Figure 3k shows that the region of enhanced positive E_N observed by THEMIS occurred near the magnetospheric edge of the current sheet, far from $B_L = 0$ (marked by the vertical red dashed line). This is consistent with the simulation finding that $E_N > 0$ at $B_L = 0$ occurs within ~2.75 d_i downstream of the X line; with a realistic proton-to-electron mass ratio, this length could be even smaller. We thus conclude that THEMIS-D probably did not encounter the electron diffusion region during this crossing.

Finally, our simulation suggests that the Larmor electric field, which was thought to be localized near the X line, extends more than 35 d_i downstream. On the other hand, signatures of magnetosheath ion gyroradius effects are more localized and are therefore better indicators of proximity (within $|L| \sim 15$ d_i) to the X line. Detection of ion gyroradius effects, however, does not imply that a spacecraft is upstream of the electron diffusion region.

Appendix A

The computational results discussed in this manuscript are from a 2.5-D collisionless antiparallel asymmetric reconnection simulation generated with the particle-in-cell (PIC) code P3D [*Zeiler et al*., 2002]. The simulation values are in physical units similar to the observations. Lengths are normalized to one ion skin depth (~59 km), based on a number density of 15 cm^{-3}. Times are normalized to one ion cyclotron time (Ω_{ci}^{-1}), which for a magnetic field of 50 nT is about 0.35 s. The speed of light in the simulation is reduced to $c_{sim} = 0.0084\,c$ which corresponds to $c_{Asheath}/c_{sim} = 0.067$ and $c_{Asphere}/c_{sim} = 0.63$, and the artificial ion to electron mass ratio is set to $m_i/m_e = 25$. The ion Larmor radius effects, which are the focus of this manuscript, are not noticeably modified by the artificially large electron mass, which we have verified by also simulating a case with $m_i/m_e = 100$. The simulation was performed over a doubly periodic domain in the L, N plane with $L \times N = 102.4 \times 51.2$ d_i, grid spacing $\Delta = 0.05$ d_i and time step $\Delta t = 0.002$ Ω_{ci}^{-1}. A density of 15 cm^{-3} at a given cell corresponds to 400 particles per cell. The simulation was initialized with a doubly asymmetric current sheet [*Malakit et al*., 2010]. The magnetosheath inflow region was initialized with a magnetic field of 30 nT, a density of 15 cm^{-3}, and ion and electron temperatures of 270 and 40 eV, respectively. The magnetospheric inflow region had a magnetic field of 50 nT, number density of 0.45 cm^{-3}, and ion and electron temperatures of 1400 eV and 52 eV, respectively. A density of 15 cm^{-3} and an electron temperature of 40 eV gives about 40 Debye lengths per ion skin depth. The simulation was evolved until it reached a steady state and then was averaged over 100 time steps spanning one ion cyclotron time to smooth the data.

Acknowledgments
Data source: THEMIS Data Center at themis.ssl.berkeley.edu. Research was supported by NSF grants AGS-1103303 and AGS-0953463 and NASA grants NNX13AD72G, NNX15AW58G, NNX08AO83G, NNX08A084G, NNX16AF75G, and NNX16AG76G. J.P.E was supported by STFC(UK) grants ST/K001051/1 and ST/N000692/1. Simulations and analysis were performed at the National Center for Atmospheric Research Computational and Information System Laboratory (NCAR-CISL) and at the National Energy Research Scientific Computing Center (NERSC).

References

André, M., A. Vaivads, S. C. Buchert, A. N. Fazakerley, and A. Lahiff (2004), Thin electron-scale layers at the magnetopause, *Geophys. Res. Lett.*, *31*, L03803, doi:10.1029/2003GL018137.

Auster, H. U., et al (2008), The THEMIS fluxgate magnetometer, *Space Sci. Rev.*, *141*(1–4), 235–264, doi:10.1007/s11214-008-9365-9.

Bonnell, J. W., F. S. Mozer, G. T. Delory, A. J. Hull, R. E. Ergun, C. M. Cully, V. Angelopoulos, and P. R. Harvey (2008), The Electric Field Instrument (EFI) for THEMIS, *Space Sci. Rev.*, *141*(1–4), 303–341, doi:10.1007/s11214-008-9469-2.

Burch, J. L., and T. D. Phan (2016), Magnetic reconnection at the dayside magnetopause: Advances with MMS, *Geophys. Res. Lett.*, doi:10.1002/2016GL069787.

Burch, J. L., et al. (2016), Electron-scale measurements of magnetic reconnection in space, *Science*, doi:10.1126/science.aaf2939.

Cassak, P. A., and M. A. Shay (2007), Scaling of asymmetric magnetic reconnection: General theory and collisional simulations, *Phys. Plasmas*, *14*, 102114, doi:10.1063/1.2795630.

Eastwood, J. P., T. D. Phan, M. Øieroset, M. A. Shay, K. Malakit, M. Swisdak, J. F. Drake, and A. Masters (2013), Influence of asymmetries and guide fields on the magnetic reconnection diffusion region in collisionless space plasmas, *Plasma Phys. Controlled Fusion*, *55*, 124001.

Egedal, J., A. Le, P. L. Pritchett, and W. Daughton (2011), Electron dynamics in two-dimensional asymmetric anti-parallel reconnection, *Phys. Plasmas*, *18*, 102901, doi:10.1063/1.3646316.

Eriksson, A. I., et al. (2006), Electric field measurements on Cluster: Comparing the double-probe and electron drift techniques, *Ann. Geophys.*, *24*, 275–289, doi:10.5194/angeo-24-275-2006.

Gosling, J. T., M. F. Thomsen, S. J. Bame, T. G. Onsager, and C. T. Russell (1990), The electron edge of low latitude boundary layer during accelerated flow events, *Geophys. Res. Lett.*, *17*, 1833–1836, doi:10.1029/GL017i011p01833.

Gosling, J. T., M. F. Thomsen, S. J. Bame, R. C. Elphic, and C. T. Russell (1991), Observations of reconnection of interplanetary and lobe magnetic field lines at the high-latitude magnetopause, *J. Geophys. Res.*, *96*, 14,097–14,106, doi:10.1029/91JA01139.

Khotyaintsev, Y., A. Vaivads, A. Retinò, M. André, C. J. Owen, and H. Nilsson (2006), Formation of the inner structure of a reconnection separatrix region, *Phys. Rev. Lett.*, *97*(20), 205003, doi:10.1103/PhysRevLett97.205003.

Khotyaintsev, Y., et al. (2016), Electron jet of asymmetric reconnection, *Geophys. Res. Lett.*, *43*, 5571–5580, doi:10.1002/2016GL069064.
Khrabrov, A. V., and B. U. Ö. Sonnerup (1998), Orientation and motion of current layers: Minimization of the Faraday residue, *Geophys. Res. Lett.*, *25*, 2373–2376, doi:10.1029/98GL51784.
Malakit, K., M. A. Shay, P. A. Cassak, and C. Bard (2010), Scaling of asymmetric magnetic reconnection: Kinetic particle-in-cell simulations, *J. Geophys. Res.*, *115*, A10223, doi:10.1029/2010JA015452.
Malakit, K., M. A. Shay, P. A. Cassak, and D. Ruffolo (2013), New electric field in asymmetric magnetic reconnection, *Phys. Rev. Lett.*, *111*, 135001, doi:10.1103/PhysRevLett.111.135001.
McFadden, J., C. W. Carlson, D. Larson, M. Ludlam, R. Abiad, B. Elliott, P. Turin, M. Marckwordt, and V. Angelopoulos (2008), The THEMIS ESA plasma instrument and in-flight calibration, *Space Sci. Rev.*, *141*(1–4), 277–302, doi:10.1007/s11214-008-9440-2.
Oieroset, M., D. Phan, J. T. Gosling, M. Fujimoto, and V. Angelopoulos (2015), Electron and ion edges and the associated magnetic topology of the reconnecting magnetopause, *J. Geophys. Res. Space Physics*, *120*, 9294–9306, doi:10.1002/2015JA021580.
Paschmann, G., B. U. Ö. Sonnerup, I. Papamastorakis, N. Sckopke, G. Haerendel, S. J. Bame, J. R. Asbridge, J. T. Gosling, C. T. Russell, and R. C. Elphic (1979), Plasma acceleration at the Earth's magnetopause: Evidence for magnetic reconnection, *Nature*, *282*, 243, doi:10.1038/282243a0.
Paschmann, G., I. Papamastorakis, W. Baumjohann, N. Sckopke, C. W. Carlson, B. U. Sonnerup, and H. Lühr (1986), The magnetopause for large magnetic shear: AMPTE/IRM observations, *J. Geophys. Res.*, *91*, 11,099–11,115, doi:10.1029/JA091iA10p11099.
Phan, T. D., G. Paschmann, and B. U. O. Sonnerup (1996), Low-latitude dayside magnetopause and boundary layer for high magnetic shear: 2. Occurrence of magnetic reconnection, *J. Geophys. Res.*, *101*, 7817–7828, doi:10.1029/95JA03751.
Phan, T. D., et al. (2003), Simultaneous Cluster and IMAGE observations of cusp reconnection and auroral proton spot for northward IMF, *Geophys. Res. Lett.*, *30*(10), 1509, doi:10.1029/2003GL016885.
Phan, T. D., et al. (2016), MMS observations of electron-scale filamentary currents in the reconnection exhaust and near the X-line, *Geophys. Res. Lett.*, *43*, 6060–6069, doi:10.1002/2016GL069212.
Shay, M. A., T. D. Phan, C. C. Haggerty, M. Fujimoto, J. F. Drake, K. Malakit, P. A. Cassak, and M. Swisdak (2016), Kinetic signatures of the region surrounding the X-line in asymmetric (magnetopause) reconnection, *Geophys. Res. Lett.*, *43*, 4145–4154, doi:10.1002/2016GL069034.
Sonnerup, B. U. Ö. (1979), Magnetic field reconnection, in *Solar System Plasma Physics*, vol. 3, edited by L. J. Lanzerotti, C. F. Kennel, and E. N. Parker, 46 pp., North Holland, Amsterdam.
Sonnerup, B. U. Ö., G. Paschmann, I. Papamastorakis, N. Sckopke, G. Haerendel, S. J. Bame, J. R. Asbridge, J. T. Gosling, and C. T. Russell (1981), Evidence for magnetic field reconnection at the Earth's magnetopause, *J. Geophys. Res.*, *86*, 10,049–10,067, doi:10.1029/JA086iA12p10049.
Tanaka, K. G., et al. (2008), Effects on magnetic reconnection of a density asymmetry across the current sheet, *Ann. Geophys.*, *26*(8), 2471, doi:10.5194/angeo-26-2471-2008.
Vaivads, A., M. André, S. C. Buchert, J.-E. Wahlund, A. N. Fazakerley, and N. Cornilleau-Wehrlin (2004), Cluster observations of lower hybrid turbulence within thin layers at the magnetopause, *Geophys. Res. Lett.*, *31*, L03804, doi:10.1029/2003GL018142.
Wilder, F. D., S. Eriksson, K. J. Trattner, P. A. Cassak, S. A. Fuselier, and B. Lybekk (2014), Observation of a retreating *x* line and magnetic islands poleward of the cusp during northward interplanetary magnetic field conditions, *J. Geophys. Res. Space Physics*, *119*, 9643–9657, doi:10.1002/2014JA020453.
Zeiler, A., D. Biskamp, J. F. Drake, B. N. Rogers, M. A. Shay, and M. Scholer (2002), Three-dimensional particle simulations of collisionless magnetic reconnection, *J. Geophys. Res.*, *107*(A9), 1230, doi:10.1029/2001JA000287.